Proceedings of the ASME 2011 International Mechanical Engineering Congress & Exposition
IMECE2011
November 11-17, 2011, Denver, Colorado, USA

IMECE2011-62018

NONCLASSICAL HEAT TRANSFER MODELS FOR LASER-INDUCED THERMAL DAMAGE IN BIOLOGICAL TISSUES

Jianhua Zhou, J. K. Chen, and Yuwen Zhang
Department of Mechanical and Aerospace Engineering
University of Missouri
Columbia, MO 65211, USA
Email: zhangyu@missouri.edu

ABSTRACT

To ensure personal safety and improve treatment efficiency in laser medical applications, one of the most important issues is to understand and accurately assess laser-induced thermal damage to biological tissues. Biological tissues generally consist of nonhomogeneous inner structures, in which heat flux equilibrates to the imposed temperature gradient via a thermal relaxation mechanism which cannot be explained by the traditional parabolic heat conduction model based on Fourier's law. In this article, two non-Fourier heat conduction models, hyperbolic thermal wave model and dual-phase-lag (DPL) model, are formulated to describe the heat transfer in living biological tissues with blood perfusion and metabolic heat generation. It is shown that the non-Fourier bioheat conduction models could predict significantly different temperature and thermal damage in tissues from the traditional parabolic model. It is also found that the DPL bioheat conduction equations can be reduced to the Fourier heat conduction equations only if both phase lag times of the temperature gradient (τ_T) and the heat flux (τ_q) are zero. Effects of laser parameters and blood perfusion on the thermal damage simulated in tissues are also studied. The result shows that the overall effects of the blood flow on the thermal response and damage are similar to those of the time delay τ_T. The two-dimensional numerical results indicate that for a local heating with the heated spot being smaller than the tissue bulk, the variations of the non-uniform distributions of temperature suggest that the multi-dimensional effects of thermal wave and diffusion not be negligible.

Keywords: Biological tissue, laser irradiation, bioheat transfer, hyperbolic thermal wave model, dual phase-lagging, protein denaturation, thermal damage.

NOMENCLATURE

A	frequency factor in the rate equation (11), s^{-1}
c	specific heat of tissues, J/(kg·K)
c_b	specific heat of blood, J/(kg·K)
E	energy of activation of denaturation reaction, J
F	light flux in seven-flux model, W/m^2
G	nisotropy factor
K	thermal conductivity of tissue, W/(m·K)
L	tissue thickness in 1-D physical model, m
$L(\bar{r},\hat{s})$	intensity of laser light at position $\bar{r}$ in the $\hat{s}$ direction, W/(m^2•sr)
$p(\hat{s},\hat{s}')$	phase function of light scattering
q	heat flux, W/m^2
$\mathbf{q}$	heat flux vector, W/m^2
q_r, q_z	radial and axial components of heat flux in cylindrical coordinates, respectively, W/m^2
Q	heat source due to other reasons, W/m^3
Q_L	heat source due to laser absorption, W/m^3
Q_m	metabolic heat generation, W/m^3
r	coordinate variable in radius direction in cylindrical coordinates, m
$\mathbf{r}$	position vector, m
R	universal gas constant, 8.314 J/(mol•K)
T	time, s
T	tissue temperature, K
T_o	initial tissue temperature, K
T_b	blood temperature, K
w_b	blood perfusion rate, m^3/(m^{3}tissue·s)
x	coordinate variable in 1-D physical model, m
z	coordinate variable in axial direction in cylindrical

coordinates, m

z_0 thickness of the cylindrical tissue, m

Greek symbols

a thermal diffusivity, m^2/s

ϕ coordinate in cylindrical coordinate system, *rad*

γ attenuation coefficient, $\gamma = \mu_a + \mu_s$, m^{-1}

μ_a absorption coefficient, m^{-1}

μ_s scattering coefficient, m^{-1}

ρ tissue mass density, kg/m^3

ρ_b blood mass density, kg/m^3

τ thermal relaxation time in hyperbolic model, s

τ_q phase lag of the heat flux, s

τ_T phase lag of the temperature gradient, s

Φ_{in} laser incident irradiance, W/m^2

$\Phi(x)$ local irradiance as a function of x, W/m^2

Ω damage integral parameter

1. INTRODUCTION

Lasers have been widely used in medical applications in the past four decades. The majority of laser medical treatments, such as laser hyperthermia, coagulation, and surgery, involve thermal effects. To improve the treatment efficiency and for personal safety, accurate analysis of thermal transport and thermal damage is of paramount importance. Most analyses are based on the well known Pennes' bioheat equation [1]:

$$\rho c \frac{\partial T}{\partial t} = \nabla \cdot (k \nabla T) + w_b \rho_b c_b (T_b - T) + Q_m + Q \qquad (1)$$

The heat conduction term in the Pennes' bioheat equation (1) is based on the classical Fourier's law.

Although the Fourier heat conduction equation is acceptable for most engineering applications, the infinite speed of thermal propagation could be inadequate in some situations; for example, those involving extremely short times, cryogenic temperatures, or high heat fluxes [2-5]. For heat transfer in biological materials with nonhomogeneous inner structures, heat flux equilibrates to the imposed temperature gradient via a relaxation mechanism [6-8]. To incorporate such a non-traditional mechanism, the Pennes' bioheat equation has been modified by including the thermal wave effects [9-12]:

$$\mathbf{q}(\mathbf{r},t) + \tau \frac{\partial \mathbf{q}(\mathbf{r},t)}{\partial t} = -k \nabla T(\mathbf{r},t) \qquad (2)$$

The theoretical value of thermal relaxation time τ in biological systems was predicted to be 20-30 s [7], and a value of approximately 16 s was experimentally observed [8]. Though the non-Fourier bioheat model [9-12] can solve the paradox of infinite thermal propagation speed, it introduces some unusual behaviors and physically impossible solutions such as negative thermal energies [13, 14].

The dual-phase lag (DPL) heat conduction model [15] introduces two time delays (alternatively called *phase lags*) to account for the two different types of delayed responses among the heat flux vector, the temperature gradient and the energy transport. Ever since its agreement with experimental results was demonstrated [16], the DPL model has attracted a considerable interest in a wide variety of scientific and engineering fields. Recently, Antaki [17] has employed the DPL heat conduction model to interpret the non-Fourier heat conduction phenomena in processed meats:

$$\mathbf{q}(\mathbf{r},t) + \tau_q \frac{\partial \mathbf{q}(\mathbf{r},t)}{\partial t} = -k\{\nabla T(\mathbf{r},t) + \tau_T \frac{\partial}{\partial t}[\nabla T(\mathbf{r},t)]\} \qquad (3)$$

where τ_T is the phase lag time for temperature gradient, and τ_q is the phase lag time for heat flux. He showed that the DPL heat conduction model correlates better with experimental data, compared to the hyperbolic thermal wave and Fourier heat conduction models.

Equation (3) shows that the temperature gradient established across a tissue volume located at a position $\mathbf{r}$ at time $t+\tau_T$ results in a heat flux to flow at a different instant of time $t+\tau_q$. For biological tissues, τ_T represents a measure of the time delay in conduction that occurs along microscopic paths (e.g. within meat particles) and τ_q is a measure of the time delay in conduction (e.g., contact resistance between different tissue constituents) [17]. Equation (3) reduces to Eq. (2) when $\tau_T = 0$ and to the classical Fourier law by further letting $\tau_q = 0$.

Currently, there exists a lot of controversy in the literature about whether or not non-Fourier conduction is important for biological tissues. Specifically, there is limited experimental evidence for this phenomenon, and some of the non-Fourier evidence has been called into question repeatedly. An excellent review on this topic can be found in [18].

Although the validity of various non-Fourier models is debatable, no ultimate conclusion has been drawn at present due to the complexity of biological systems. Recently, some physical anomalies concerning the DPL model have been reported for several particular cases [19]. Nevertheless, because the dual-phase-lag model offers the possibility to conveniently capture----at macroscale level----some microscale processes of conduction, it has attracted a great deal of attention over the last ten years. For example, Xu et al. [20] derived the bioheat equation in the vector format and used the derived equation to study the 1D thermal damage of skin.

In this article, the heat conduction and thermal damage in laser-irradiated biological tissues are investigated using non-Fourier heat conduction model. The hyperbolic thermal wave and dual-phase-lag constitutive equations are incorporated into the bioheat transfer model in living tissues. Comparisons among the results obtained by the traditional parabolic model, thermal wave model and DPL model are made. Some important aspects involved in the non-Fourier descriptions of the heat transfer in living biological tissues are discussed and identified.

2. PHYSICAL MODEL

In this work, the 2-D axisymmetric hyperbolic thermal wave model, 1-D DPL model and 2-D axisymmetric DPL model will be formulated to describe the non-Fourier heat conduction phenomena in laser-irradiated biological tissues.

The physical model and finite difference mesh for the 1-D DPL analysis are shown in Figure 1. A finite slab of biological tissue with a thickness of L and initial temperature T_0 is considered. At time $t = 0^+$, a broad laser beam with a uniform irradiance (Φ_{in}) is applied normally to the left surface. When the spot size of the broad laser beam is much larger than the thickness of the thermally affected zone for the time period of interest, a one-dimensional (1-D) model would be sufficient for analyzing the thermal response of the heated medium. The right boundary surface is considered to be thermally insulated to the environments (q = 0), while the boundary condition at the left (irradiated) surface is specified depending on the irradiation penetration depth of the laser beam.

The physical model and mesh for the 2-D hyperbolic thermal wave model and 2-D DPL model are shown in Figure 2. We consider a cylindrical biological tissue of radius r_o and thickness z_o irradiated by electromagnetic waves normally to the left surface (z= 0) over a circular spot of radius r_p for a time period t_p. The living tissue is initially at a uniform temperature T_o. Assume that the irradiation is uniform or in a Gaussian distribution. The thermal load can be modeled as a surface heat flux or a body heat source, depending on the irradiation penetration depth. Let the center of the incident heat flux (Φ_{in}) coincide with the origin O of the cylindrical coordinate system. The other boundary surfaces are assumed to be thermally insulated. Due to the axisymmetry of the tissue geometry and the thermal load, only a 2D axisymmetric cylindrical domain $OABC$ (Fig. 2 (a)) needs to be analyzed for the thermal transfer in the tissue. The 2-D mesh is shown in Fig. 2 (b).

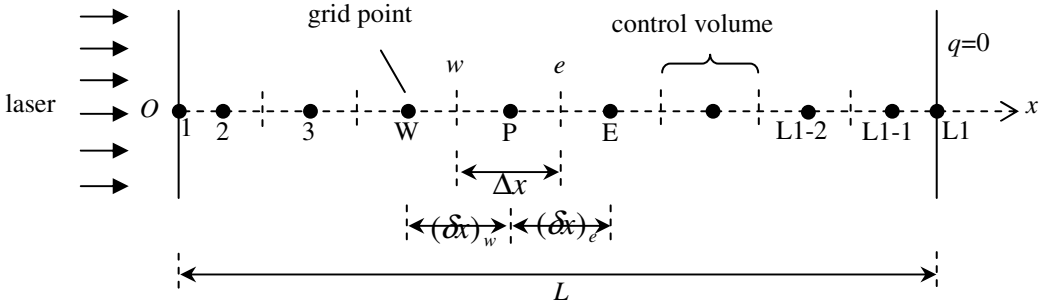

Figure 1 Physical model and grid system for 1-D analysis

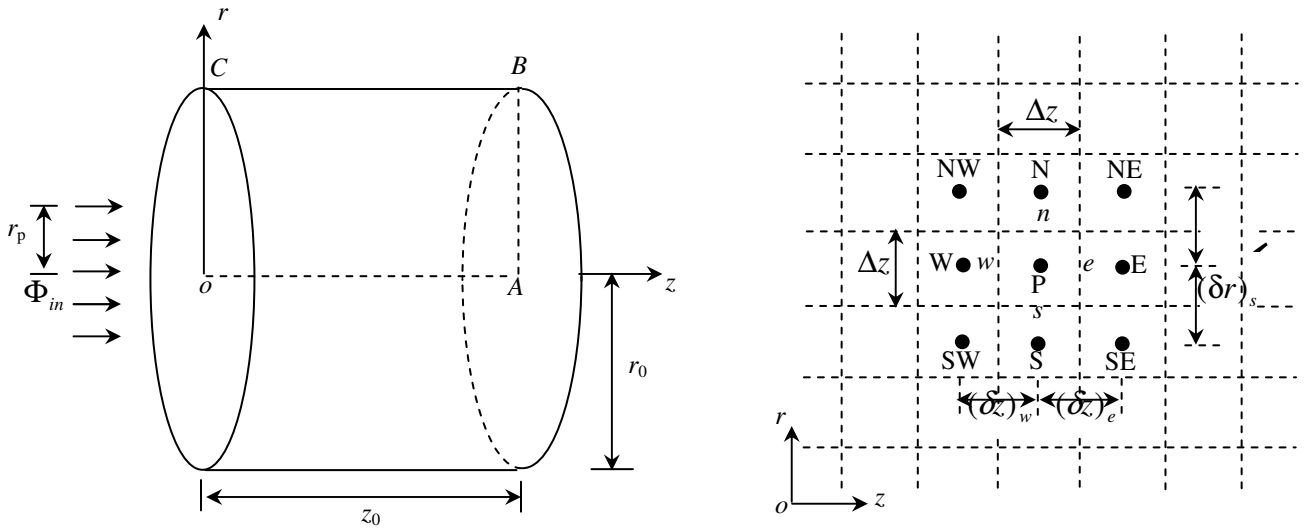

Figure 2 Physical model and grid system for 2-D analysis
(a) physical model; (b) grid system.

3. MATHEMATICAL FORMULATION

3.1 Bioheat transfer model

3.1.1 2-D axisymmetric hyperbolic thermal wave model

The 2D axisymmetric thermal wave model of bioheat transfer equation in laser-irradiated tissues and two heat flux constitutive relations can be written as follows:

$$\rho c\frac{\partial T}{\partial t}=-\frac{1}{r}\left[\frac{\partial(r\cdot q_r)}{\partial r}+\frac{\partial(r\cdot q_z)}{\partial z}\right]+w_b\rho_b c_b(T_b-T)+Q_m+Q_L \quad (4)$$

$$\tau\frac{\partial q_z}{\partial t}+q_z=-k\frac{\partial T}{\partial z} \quad (5)$$

$$\tau\frac{\partial q_r}{\partial t}+q_r=-k\frac{\partial T}{\partial r} \quad (6)$$

The heat generation due to laser absorption will be addressed later. Equations (4)-(6) reduce to the classical Fourier model when the relaxation time $\tau = 0$. We assume that all the boundaries are thermally insulated. The tissue is regarded as a turbid scattering one, and thus the laser heating is considered as a body heat source.

To capture the thermal wave phenomena, the oscillation-free total variation diminishing method [21], a highly accurate and stable approach, is employed for the numerical analysis. The implementation of this high accurate approach in cylindrical coordinate system is available in [22].

3.1.2 1-D DPL model

The 1-D bioheat equation in laser-irradiated tissues considering blood perfusion and metabolic heat generation is as follows:

$$\rho c\frac{\partial T}{\partial t}=-\frac{\partial q}{\partial x}+w_b\rho_b c_b(T_b-T)+Q_m+Q_L \quad (7)$$

Combining Eqs. (3) and (7) while eliminating the heat flux q lead to the following 1-D DPL bioheat conduction equation for tissue temperature $T(x,t)$:

$$\tau_q\frac{\partial^2 T}{\partial t^2}+(1+\frac{w_b\rho_b c_b}{\rho c}\tau_q)\frac{\partial T}{\partial t}=\alpha\frac{\partial^2 T}{\partial x^2}+\alpha\tau_T\frac{\partial^3 T}{\partial t\partial x^2}+\frac{Q_L}{\rho c}+\frac{Q_m}{\rho c}+\frac{w_b\rho_b c_b}{\rho c}(T_b-T) \quad (8)$$

Alternatively, combining Eq. (3) and (7) while eliminating T gives the DPL bioheat conduction equation for heat flux $q(x,t)$:

$$\tau_q\frac{\partial^2 q}{\partial t^2}+\frac{\partial q}{\partial t}=\alpha\frac{\partial^2 q}{\partial x^2}+\alpha\tau_T\frac{\partial^3 q}{\partial t\partial x^2}-\alpha\frac{\partial Q_L}{\partial x}+\alpha w_b\rho_b c_b\frac{\partial T}{\partial x}+\alpha w_b\rho_b c_b\tau_T\frac{\partial^2 T}{\partial t\partial x} \quad (9)$$

In this study, Eq. (9) will be used as the basic governing equation to simulate the DPL heat conduction in tissue since it is more convenient to solve the problems involving heat flux specified boundary conditions. The laser irradiation will be treated in two different ways. For highly absorbed tissues, the surface laser heating will be approximated as the second kind of boundary condition. For strongly scattering tissues, the laser heating is considered as a body heat source and correspondingly, the irradiated surface is regarded as being thermally insulated.

3.1.3 2-D DPL model

The bioheat equation for laser-irradiated tissues in vector form is given by:

$$\rho c\frac{\partial T}{\partial t}=-\nabla\bullet\mathbf{q}+w_b\rho_b c_b(T_b-T)+Q_m+Q_L \quad (10)$$

Combining the energy balance equation (10) and the dual-phase-lag constitutive relation Eq. (3) while eliminating the heat flux $\mathbf{q}$ leads to the following DPL bioheat conduction equation for tissue temperature:

$$\tau_q\frac{\partial^2 T}{\partial t^2}+(1+\frac{w_b\rho_b c_b}{\rho c}\tau_q)\frac{\partial T}{\partial t}=\alpha\nabla\bullet(\nabla T)+\alpha\tau_T\frac{\partial}{\partial t}[\nabla\bullet(\nabla T)]+\frac{w_b\rho_b c_b}{\rho c}(T_b-T)+\frac{w_b\rho_b c_b\tau_q}{\rho c}\frac{\partial T_b}{\partial t}+\frac{Q_m+Q_L}{\rho c}+\frac{\tau_q}{\rho c}(\frac{\partial Q_m}{\partial t}+\frac{\partial Q_L}{\partial t}) \quad (11)$$

Like the 1-D case, the DPL bioheat conduction equation can also be derived for heat flux $\mathbf{q}(\mathbf{r},t)$ by eliminating the temperature T:

$$\frac{\partial\mathbf{q}}{\partial t}+\tau_q\frac{\partial^2\mathbf{q}}{\partial t^2}=\alpha\nabla(\nabla\bullet\mathbf{q})+\alpha\tau_T\frac{\partial}{\partial t}[\nabla(\nabla\bullet\mathbf{q})]+\alpha w_b\rho_b c_b(\nabla T-\nabla T_b)+\alpha\tau_T w_b\rho_b c_b\frac{\partial}{\partial t}(\nabla T-\nabla T_b)-\alpha(\nabla Q_m+\nabla Q_L)-\alpha\tau_T[\frac{\partial}{\partial t}(\nabla Q_m+\nabla Q_L)] \quad (12)$$

In the derivations of Eqs. (11) and (12), all the thermal properties are assumed to be constant.

In this study, the heat flux formulation of the DPL bioheat conduction, i.e., Eq. (12), is adopted for analyzing the heat conduction in the 2-D cylindrical living tissue shown in Fig. 2(a).

The blood temperature T_b and the metabolic heat generation Q_m in Eq. (12) are assumed to be constant for emphasizing the essential physics of the DPL bioheat transfer. Under this assumption, those terms with the gradients of T_b and Q_m can be dropped off from Eq. (12). Accordingly, the two axisymmetric equations governing the heat transfers in the r- and x-direction can be expressed from Eq. (12):

$$\frac{\partial q_r}{\partial t}+\tau_q\frac{\partial^2 q_r}{\partial t^2}=\alpha\frac{\partial}{\partial r}\{\frac{1}{r}[\frac{\partial(rq_r)}{\partial r}+\frac{\partial(rq_z)}{\partial z}]\}+\alpha\tau_T\frac{\partial^2}{\partial r\partial t}\{\frac{1}{r}[\frac{\partial(rq_r)}{\partial r}+\frac{\partial(rq_z)}{\partial z}]\}+\alpha w_b\rho_b c_b\frac{\partial T}{\partial r}+\alpha w_b\rho_b c_b\tau_T\frac{\partial^2 T}{\partial r\partial t}-\alpha\frac{\partial Q_L}{\partial r}-\alpha\tau_T\frac{\partial^2 Q_L}{\partial r\partial t} \quad (13)$$

$$\frac{\partial q_z}{\partial t}+\tau_q\frac{\partial^2 q_z}{\partial t^2}=\alpha\frac{\partial}{\partial z}\{\frac{1}{r}[\frac{\partial(rq_r)}{\partial r}+\frac{\partial(rq_z)}{\partial z}]\}+\alpha\tau_T\frac{\partial^2}{\partial z\partial t}\{\frac{1}{r}[\frac{\partial(rq_r)}{\partial r}+\frac{\partial(rq_z)}{\partial z}]\}+\alpha w_b\rho_b c_b\frac{\partial T}{\partial z}+\alpha w_b\rho_b c_b\tau_T\frac{\partial^2 T}{\partial z\partial t}-\alpha\frac{\partial Q_L}{\partial z}-\alpha\tau_T\frac{\partial^2 Q_L}{\partial z\partial t} \quad (14)$$

The specification of the boundary conditions is similar to that in the case of 1-D DPL model.

3.2 Light propagation

When laser irradiation is highly absorbed by a tissue (e.g. for some UV and IR wavelengths), the laser light can be absorbed within an extreme small depth, say on the ~μm order of magnitude. For such a case, laser heating can be reasonably approximated by considering the laser irradiance as a surface

heat flux on the irradiated boundary. For the cases that scattering is significant over the visible and near-infrared wavelengths [23], laser energy deposition into a tissue cannot be simply described as a heat flux boundary condition. Instead, the laser light attenuation in the tissue needed to be determined with knowledge of optical properties and light propagation. The resulting spatially varied Q_L then serves as a body heat source that heats up the tissue.

A radiation transfer integral equation for laser light propagation in biological tissues is given by [23]

$$\hat{s}\cdot\nabla L(\bar{r},\hat{s})+\gamma L(\bar{r},\hat{s})=\frac{\gamma}{4\pi}\int_{4\pi}p(\hat{s},\hat{s}')L(\bar{r},\hat{s}')d\omega' \qquad (15)$$

where $\bar{r}$ is a position vector, $\hat{s}$ and $\hat{s}'$ are the direction vectors, $L(\bar{r},\hat{s})$ is the intensity of laser light at position $\bar{r}$ in the $\hat{s}$ direction, ω' is the solid angle, and $p(\hat{s},\hat{s}')$ is the phase function representing the scattering contribution from $\hat{s}'$ to the $\hat{s}$ direction. The unit of L in Eq. (15) is W/m^2−sr. The solid angle integration of the phase function is defined as

$$\frac{1}{4\pi}\int_{4\pi}p(\hat{s},\hat{s}')d\omega'=\frac{\mu_s}{\gamma} \qquad (16)$$

where the attenuation coefficient γ is the sum of the absorption coefficient (μ_a) and the scattering coefficient (μ_s).

The exact analytical solutions of Eq. (15) are only available for limited cases, therefore, some approximation approaches are developed to calculate the light propagation in tissues.

3.2.1 Beer's law

The simplest approximation of laser deposit in tissues is Beer's law. The volumetric heat source due to laser absorption can be written as:

$$Q_L=\mu_a\cdot\Phi_{in}\exp(-\mu_a x) \qquad (17)$$

where μ_a denotes the effective absorption coefficient. Φ_{in} is the incident intensity of the laser irradiation.

3.2.2 Broad beam method

The broad beam irradiation method [24] can also be adopted to calculate the laser energy deposition in scattering tissues. The laser irradiance $\Phi(x)$ is expressed as:

$$\Phi(x)=\Phi_{in}[C_1\exp(-k_1x/\delta)-C_2\exp(-k_2x/\delta)] \qquad (18)$$

where C_1, k_1, C_2, k_2 are parameters that are determined based on the Monte Carlo solutions, depending on the diffuse reflectance; δ is the effective optical penetration depth, which is defined from the diffusion theory as:

$$\delta=\frac{1}{\sqrt{3\mu_a[\mu_a+\mu_s(1-g)]}} \qquad (19)$$

where μ_s is the scattering coefficient; g is the anisotropy factor. A reduced scattering coefficient is usually introduced as $\mu_s'=\mu_s(1-g)$ for convenience.

Once the light irradiance distribution in the tissue is determined from Eq. (18), the laser volumetric heat source Q_L can be calculated by:

$$Q_L(x)=\mu_a\Phi(x) \qquad (20)$$

3.2.3 Seven flux model

The seven-flux model proposed by Yoon et al. [25], on the other hand, is an accurate and fast algorithm for computing laser light distribution in tissues, in which the differential-integral equation (15) can be converted to a linear system of equations.

The governing equations for the seven fluxes in a cylindrical coordinate system (r, z, ϕ), depicted in Fig. 2 (a), are expressed as follows [26]:

$$\frac{\partial F_c(r,z,\phi)}{\partial z}=-\gamma F_c(r,z,\phi) \qquad (21)$$

$$\frac{\partial F_{x_i}(r,z,\phi)}{h\partial x_i}+\gamma F_{x_i}=\gamma[p_{x_i,+r}F_{+r}+p_{x_i,-r}F_{-r}+p_{x_i,+\phi}F_{+\phi}+p_{x_i,-\phi}F_{-\phi}+p_{x_i,+z}F_{+z}+p_{x_i,-z}F_{-z}+p_{x_i,+z}F_c] \qquad (x_i=\pm r,\pm z,\pm\phi) \qquad (22)$$

where F_c is the collimated light flux in the +z direction; $F_{\pm r}$, $F_{\pm z}$ and $F_{\pm\varphi}$ are the six components of the scattered light flux in the $\pm r$, $\pm z$ and $\pm\phi$ directions, respectively; $h=1, 1, r$ for $x_i=\pm r,\pm z,\pm\phi$, respectively; the phase function $p(\hat{s},\hat{s}')$ in Eq. (15) is represented by p_{ij}, denoting the portion of the flux scattered from the j-direction into the i-direction. Because of the axisymmetric nature considered here, the fluxes in the $\pm\phi$ directions are identical. Thus, the number of the governing equations (22) reduces to 5. Detailed description for determination of p_{ij} can be found in References [26].

3.3 Damage prediction

To quantify the extent of thermal damage in a living tissue, a damage parameter Ω is defined as [27]:

$$\Omega=\ln\left(\frac{C_0}{C_0-C_d}\right) \qquad (23)$$

where C_0 is the protein concentration in the non-irradiated tissue, C_d is the concentration of denaturated protein. The protein denaturation process is considered as a chemical reaction. The damage parameter Ω is evaluated according to the Arrenius equation [27]:

$$\Omega=A\int_{t_1}^{t_f}\exp\left(-\frac{E}{RT}\right)dt \qquad (24)$$

where A is the frequency factor; E is the energy of activation of denaturation reaction; R is the universal gas constant, 8.314 J/(mol•K); T is the absolute temperature of the tissue at the point where Ω is calculated; t_1 is the time at the onset of laser exposure; t_f is the time when the thermal damage is evaluated.

Numerical values for the frequency factor and the activation energy are given as: $A = 3.1\times10^{98}$ s^{-1}; $E = 6.28\times10^5$ J/mol [27]. The tissue is assumed to be irreversible damaged

when Ω = 1.0 [27], which corresponds to a denaturation of 63% of the molecules.

4. VERIFICATION OF COMPUTER CODES

The finite difference computer codes have been written based on the mathematical formulations as previously described. In the following, these computer codes will be verified with several test problems.

4.1 2-D thermal wave model of bioheat transfer

The computer code for the thermal wave model is validated with a test problem, where the radius and thickness of the 2D axisymmetric cylinder (Fig. 2(a)) are 5 mm. The initial temperature of the cylinder is uniform at 20 ºC. The blood perfusion and metabolic terms are temporally turned off. At time $t = 0$, the left surface ($z = 0$) of the cylinder is subjected to a Gaussian irradiance with a peak intensity of 3000 W/m^2 for 5 s. The radius of the cross section of the heat flux is $r_p = 2$ mm. The physical properties of the cylindrical biological tissue are the same as in reference [28]. For comparison, a 2D axisymmetric traditional parabolic model is also used. Figure 3(a) shows the comparison for the time histories of temperature at the origin (0,0), calculated from the thermal wave and traditional parabolic models. It is seen from Fig. 3(a) that thermal wave characteristics are clearly exhibited for higher values of thermal relaxation time τ. As τ decreases, the thermal wave model asymptotically approaches the traditional parabolic model. The above numerical test shows that the algorithms employed in the present approach give reliable and non-oscillatory results.

4.2 1-D DPL model

Consider a 1-D slab as shown in Fig. 1. All the parameters are non-dimensionalized. For comparison, the thermal parameters and the geometries are chosen to be the same as those reported in reference [15]. The dimensionless thickness of the slab is 1. Both the initial temperature and the initial time-rate change of temperature are zero. At time $t = 0^+$, the left surface at $x = 0$ is suddenly raised to a temperature $T_w = 1$ while the right surface at $x = 1$ remains at a zero temperature gradient. Since there is no internal heat source in this test problem, the laser-induced heat distribution, blood perfusion and metabolic heat generation are dropped from the governing equation. The temperature formulation (Eq. (8)) and the heat flux formulation (Eq. (9)) take the same form when internal heat sources are excluded.

Figure 3(b) shows the spatial distributions of temperature at time $t = 0.05$. In these calculations the value of τ_q is maintained at 0.05 while the value of τ_T varies from 0.001 to 0.5. It appears that the present DPL model calculations agree very well with the analytical solutions [15]. The thermal wave characteristic becomes pronounced for very small τ_T, 0.001 in Fig. 3(b). When τ_T is equal to τ_q (see $\tau_T = \tau_q = 0.05$ in Fig. 3(b)), the DPL model reduces to the Fourier heat conduction theory.

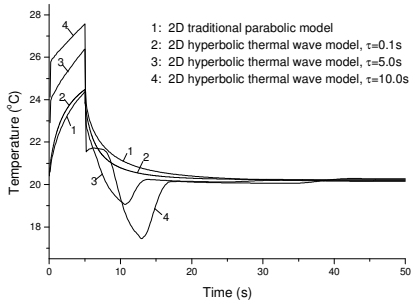

(a)

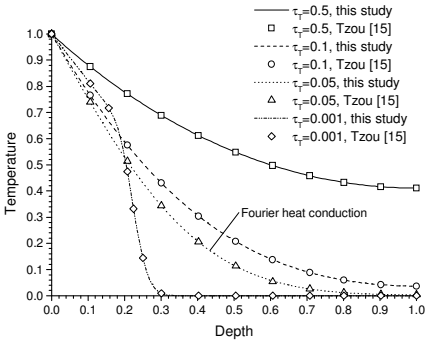

(b)

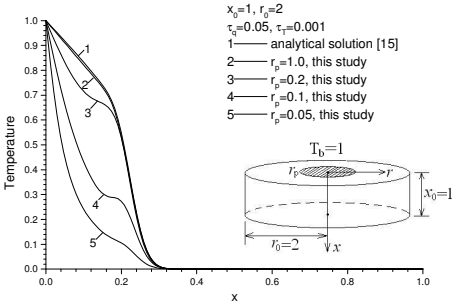

(c)

Figure 3 Verification of computer code. (a) 2-D hyperbolic thermal wave model; (b) 1-D DPL model; (c) 2-D DPL model.

4.3 2-D DPL model

The simulation model is the same as that shown in Fig. 2(a). The difference is that the left surface of the cylinder is subject to a first kind of boundary condition rather than laser heating. To keep consistency with the analytical solution presented in [15], the numerical simulation is performed based on dimensionless quantities. The thickness and the radius of the cylinder are z_0=1 and r_0=2, respectively. Initially, the cylinder is uniformly at the temperature of T_0=0. From time t>0, the temperature of a finite circular area (whose center is located at (0,0)) at the left surface of the cylinder is elevated to T_b=1. The radius of the finite heating area is denoted by r_p, which changes from 0.05 to 1.0. Other boundaries of the cylinder remain at zero temperature gradient. The temperature formulation of the

2D DPL model (i.e., Eq. (11)) will be used to simulate this test problem. The blood perfusion and metabolic heat generation are turned off in order to make our numerical simulation results comparable with analytical solution [15]. Other simulation parameters (which are also non-dimensional) are as follows: thermal diffusivity $\alpha = 1$, phase lag time of heat flux $\tau_q = 0.05$, phase lag time of temperature $\tau_T = 0.001$.

Figure 3(c) shows the spatial distribution of temperature along the cylinder centerline (r=0) at time t=0.05. It can be clearly seen that the 2D temperature distribution gradually approaches the 1D analytical solution [15] when the heating spot size rp is increased from 0.05 up to 1.0. When the heating spot size becomes equal to the thickness of the cylinder (i.e., r_p=1.0, curve 2 in Fig.3), the calculating results are almost the same as the analytical solution [15]. This indicates that when the heating spot radius is increased up to the thickness of the cylinder, the 2D DPL heat conduction in the cylinder is close to 1D heat conduction. The calculating results presented in Fig. 3(c) justify the credibility and reliability of the 2D DPL numerical model developed in this study.

5. RESULTS AND DISCUSSION

When the tissue temperature is elevated to as high as 100°C, phase change will take place and the tissue can be vaporized. During this stage, pure heat conduction models may not be able to describe the complex heat transfer process. The simulation parameters employed in this study are chosen to make sure that the tissue temperature will not exceed 100°C. The cases studied in this work may find its potential applications in laser hyperthermia or laser coagulation therapy.

Unless otherwise mentioned, the following properties [28] of a biological tissue are used in the following numerical analysis: ρ = 1000 kg/m^3, k = 0.628 W/(m·K), c = 4187 J/(kg·K) for the thermophysical properties; ρ_b = 1.06×10^3 kg/m^3, c_b = 3860 J/(kg·K), w_b = 1.87×10^{-3} m^3/(m^{3}tissue·s), T_b = 37 °C, Q_m = 1.19×10^3 W/m^3 for the thermal physical properties and temperature of blood and the metabolic heat generation, respectively. The two phase lag times τ_T and τ_q are ranged from 0 s∼32 s, which are based on the previous studies [7, 8, 14].

Figure 4 shows the time histories of temperature T and the damage parameter Ω at the irradiated surface for the 1-D DPL model case that laser light is highly absorbed in tissue. As previously stated, for this case, the second kind of boundary condition can be applied at the laser irradiation surface. The physical model is shown in Fig.1. The thickness of the slab tissue is 5 cm, and the initial temperature is T_0 = 37 °C. The incident laser irradiance is 2 W/cm^2. The diffuse reflectance is considered as 5%, which means only 95% of the incident laser irradiance enters the tissue. The duration time of laser irradiation is 5 s. The lag times used in the computation are $\tau_q = 16.0\ s$ and $\tau_T = 0.05\ s$ for the DPL model, $\tau_q = 16.0\ s$ for the hyperbolic thermal wave model, and $\tau_T = \tau_q = 0$ for the Fourier heat conduction model. Figure 4(a) compares the transient temperature responses obtained from the Fourier heat conduction, themal wave, and DPL models, and Figs. 4(b)~(d) display the change of the resulting damage parameters. As shown in Fig.4, the thermal wave model not only predicts the highest temperature rise compared to the other two models, but results in the quickest tissue irreversible damage as well. However, the DPL bioheat transfer model predicts a moderate temperature rise compared to the hyperbolic heat conduction model. On the other hand, the traditional parabolic heat conduction model predicts the lowest temperature rise. This is because the Fourier model assumes an infinite propagation speed of heat. Upon the laser beam impinges onto the tissue surface, the heat is transferred into deep tissues without any delay. The results in Fig. 4 indicate that, the tissue damage predicted with the temperature computed with the traditional parabolic model could be conservative. This suggests that the bioheat non-Fourier effect be taken into account in prediction of laser-induced thermal damage. Otherwise, the damage assessment may not be reliable.

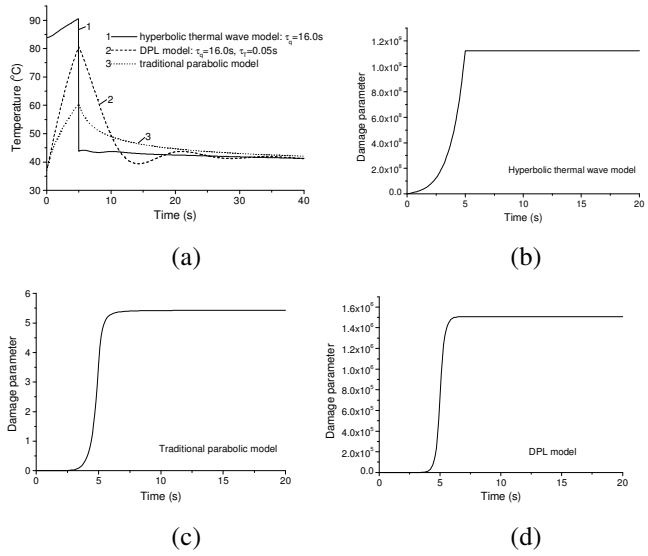

Figure 4 Temporal evolution of temperature and thermal damage at the irradiated surface of a highly absorbing tissue simulated by hyperbolic thermal wave, DPL and traditional parabolic models: (a) temperature and (b)~(d) damage parameter.

In a scattering-dominated tissue, the laser irradiation should be considered to be a volumetric heat source based on the calculation of light propagation. Figure 5 illustrates the temperature and damage transients at irradiation surface in the scattering-dominated tissue for 1-D DPL model. The phase lag times used in this analysis are the same as those in the previous case (Fig. 4). The laser irradiance is increased to 30 W/cm^2. The light propagation is computed using the broad beam approach. The optical properties are: μ_s = 120.0 cm^{-1}, μ_a =0.4 cm^{-1}, g = 0.9. It is observed from Fig. 5 that the results

obtained from the hyperbolic thermal wave model ($\tau_q = 16.0\ s$) are almost identical to that obtained from the DPL model ($\tau_q = 16.0\ s$, $\tau_T = 0.05\ s$). The Fourier heat conduction model still results in the lowest temperature rise and mildest thermal damage.

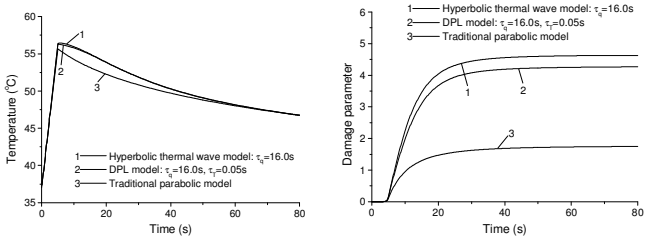

(a) (b)

Figure 5 Temporal evolution of temperature and thermal damage at the irradiated surface of a scattering tissue simulated by hyperbolic thermal wave, DPL and traditional parabolic models: (a) temperature and (b) damage parameter.

The results presented in Fig. 5 is for two particular cases where the thermal relaxation time τ_q is assumed to be 16 s for the hyperbolic thermal wave model and the two phase lags τ_q and τ_T are assumed to be 16 s and 0.05 s for the DPL model. In reality, the non-homogeneous inner structures in tissues are different from one body part to another. This means that the two phase lags τ_q and τ_T may vary over a wide range. The influences of the τ_q and τ_T on the temperature and damage responses are presented in Figure 6. Figs. 6(a) and (b) show the temporal evolutions of temperature *T* and the damage parameter Ω at the irradiation surface calculated by the 1-D DPL model with $\tau_q = 16.0\ s$ and different values of τ_T. The incident irradiance of the laser beam is set at 30 W/cm^2. As seen from Fig. 6(a), the temperature transients during the laser irradiation time period (5 s here) are almost the same for different τ_T values. However, the temperatures become diverse for different τ_T values after the laser is turned off. This leads to a different damage progress, and, in turn, results in different final damage extents in the tissue (see Fig. 6(b)). The longer the phase lag τ_T, the larger the saturated value of the damage parameter. The saturated damage parameter Ω predicted with $\tau_T = 32$ s is about 3.5 times that predicted by the Fourier heat conduction model. It is noticed from Fig. 6(a) that the temperature transient computed with $\tau_q = \tau_T = 16.0$ s (curve 2 in Fig. 6(a)) is not the same as the result of the Fourier heat conduction model (curve 5 in Fig. 6(a)). This is in contrast to the result for pure conduction media where the DPL model will approach the Fourier model when $\tau_q = \tau_T$ [15]. The discrepancy results from the blood perfusion. It can be seen from Eqs. (8) and (9) that the presence of the blood perfusion leads to an extra term involving with τ_q in the temperature formulation (the second term in the parenthesis on the right hand side of Eq. (8)) and an extra term involving with τ_T in the heat flux formulation (the last term in Eq. (9)). Under this circumstance, the DPL bioheat conduction equations can be reduced to the Fourier heat conduction equations only if both τ_q and τ_T are zero.

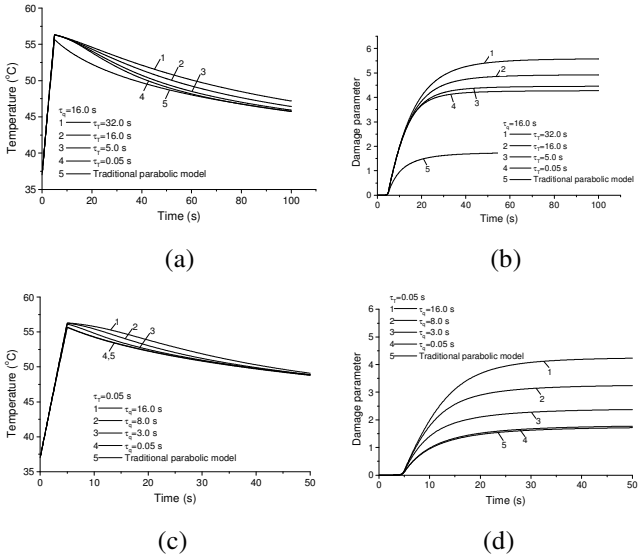

(a) (b)

(c) (d)

Figure 6 Influences of the τ_q and τ_T on the temperature and damage responses. (a) temperature response at the irradiated surface for different τ_T values while τ_q is fixed; (b) damage response at the irradiated surface for different τ_T values while τ_q is fixed; (c) temperature response at the irradiated surface for different τ_q values while τ_T is fixed; (d) damage response at the irradiated surface for different τ_q values while τ_T is fixed.

Figures 6 (c) and (d) illustrate the effect of τ_q on the transient evolutions of the surface temperature and damage parameter. It is found that the longer the time delay τ_q is, the higher the temperature rise and the larger the saturated value of the damage parameter. When τ_q decreases to 0.05s, the curve of the temperature transients almost overlap with that obtained by the Fourier heat conduction equation (curves 4 and 5 in Fig. 6(c)). Comparing the temperature results in Figs. 6(a) and 6(c) shows that for laser-irradiated biological tissues τ_q has more impact on the temperature in the early time while τ_T has more impact on the temperature in the late time. The DPL results will approach the traditional Fourier heat conduction results only when both τ_T and τ_q are very small. Otherwise, the heat conduction described by the DPL bioheat transfer model would

differ from the traditional Fourier bioheat model even if $\tau_T = \tau_q$.

Tissue vasclature plays an important role in laser-induced thermotherapy. An optimized treatment procedure cannot be obtained without carefully evaluating the convective cooling effect of the blood flow. Blood perfusion rates are quite different for different body parts and physiological conditions. The effect of the blood perfusion rate on the temperature and thermal damage is demonstrated in Figure 7. As expected, the higher the blood perfusion rate, the stronger the convection heat loss due to faster blood flow, and the less extent the thermal damage. It is found, by comparing the results in Figs. 6(a),(b) and 7, that the overall effect of the blood flow is similar to that of the time delay τ_T. As mentioned previously, τ_T is the delay in establishing the temperature gradient across the tissue during which conduction occurs through its small-scale structures. The heat exchange between capillary blood vessels and tissues will considerably reduce the magnitude of temperature gradient in the bulk medium.

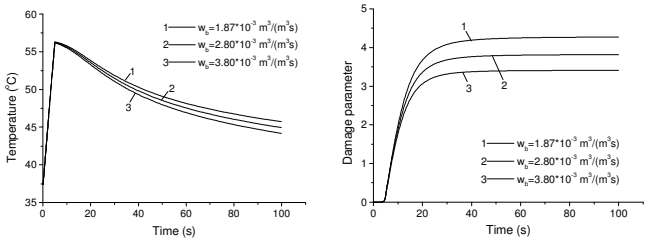

(a) (b)

Figure 7 Effects of blood perfusion rate on temperature and thermal damage at the irradiated surface of a scattering tissue.

The optical properties could vary significantly from one tissue to another [29], thereby resulting in different temperature field and subsequently causing different thermal damage. Figure 8 shows the effects of light scattering in the tissue on the temperature response and damage parameter at the point (0,0) for a 2-D thermal wave model. The light transportation is simulated using the seven flux model. As shown in Figs. 8 (a) and (b), both the temperature and damage parameter increase as the scattering coefficient increases, leading to more severe damage. Figure 8 also shows that the increases in both temperature and damage parameter become more slowly when the scattering coefficient further increases.

Distribution of the saturated damage parameter over the analyzed domain is plotted in Figs. 8(c) and (d) for two scattering coefficients μ_s = 5 cm^{-1} and 10.6 cm^{-1}, respectively. Obviously, thermal damage could be more serious for a tissue having a higher scattering coefficient. However, there is no considerable change in the total volume of the thermally damaged tissue for the two scattering coefficients.

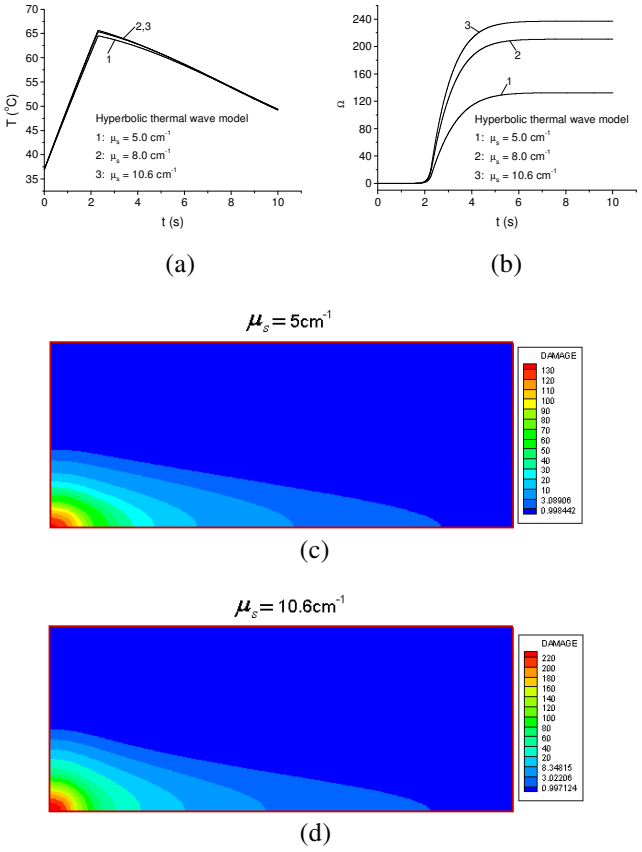

(a) (b)

(c)

(d)

Figure 8 Effects of scattering coefficient (μ_s) on temperature and damage at point (0,0). (a) temperature at (0,0) as a function of time; (b) damage at (0,0) as a function of time; (c) distribution of damage parameter for $\mu_s = 5cm^{-1}$; (d) distribution of damage parameter for $\mu_s = 10.6cm^{-1}$.

Figure 9 illustrates the effect of tissue absorption coefficient on the temperature and thermal damage at the point (0,0). It can be seen from Figs. 9(a) and (b) that the larger the absorption coefficient, the earlier and steeper the damage parameter rise and the greater the saturated value. This is attributed to more laser energy absorbed in the subsurface layer of the tissue due to the smaller optical penetration depth (the larger absorption coefficient). As a result, the resulting temperature is higher and, in turn, thermal damage becomes more severe in this thin layer. The same trend can also be seen in Figs. 9(c) and (d). Unlike the tissue scattering coefficient, the total volume of the damage tissue can be enlarged remarkably, besides the escalation in the degree of tissue damage.

For a local heating with the heated spot being smaller than the tissue bulk, the variations of the non-uniform distributions of temperature suggest that the multi-dimensional effects of thermal wave and diffusion not be negligible. For this case, the 1-D model is inadequate. Figure 10 compares the temperature

distributions calculated by the 2-D DPL and 2-D Pennes bioheat conduction models. The phase lag times used here are τ_q = 8 s and τ_T = 0.5 s. In this calculation, the boundary condition of the second kind is applied for a surface heating with a constant heat flux Φ_{in} = 4 W/cm^2 and r_p = 1 cm. It can be seen from Figs. 10 (a)-(d) that the thermal wave response, simulated by the 2-D DPL bioheat conduction model, occurs in both the axial (Fig. 10 (b)) and radial (Figs. 10 (b)-(d)) directions. On the other hand, the classical Pennes' bioheat model leads to smooth temperature distributions (Figs. 10 (e)-(f)). The transients of the tissue temperature, particularly in the region near the heated spot edge, shown in Fig. 10 manifest the inadequacy of the 1D approach.

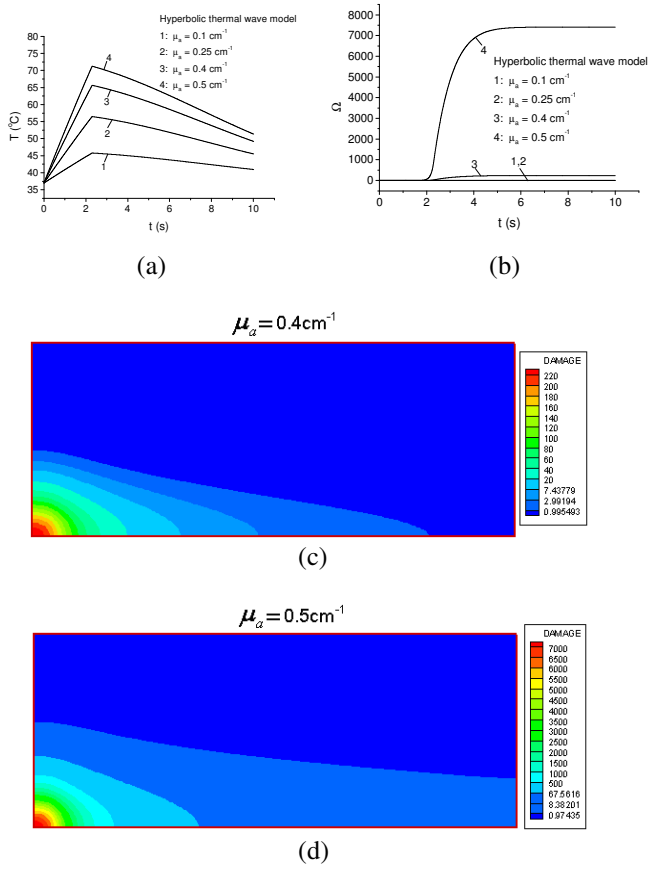

Figure 9 Effects of absorption coefficient (μ_a) on temperature and damage at point (0,0). (a) temperature at (0,0) as a function of time; (b) damage at (0,0) as a function of time; (c) distribution of damage parameter for $\mu_a = 0.4cm^{-1}$; (d) distribution of damage parameter for $\mu_a = 0.5cm^{-1}$.

Figure 11 shows 2-D temperature distributions at four different time instants for the tissue subjected to a body heating. In this simulation, a uniform irradiation of intensity Φ_{in} = 150 W/cm^2 is impinging on the top surface x = 0 over a circular spot of r_p = 2 cm. The volumetric heat source is assumed to follow the Beer's law with the effective absorption coefficient μ_a = 1 cm^{-1}. As is seen, the resulting temperature distribution in the axial direction is less steep and no thermal wave is found. However, thermal wave does exhibit in the radial direction due to the sharp temperature variation at the heated spot edge (Figs. 11 (c) and 11 (d)).

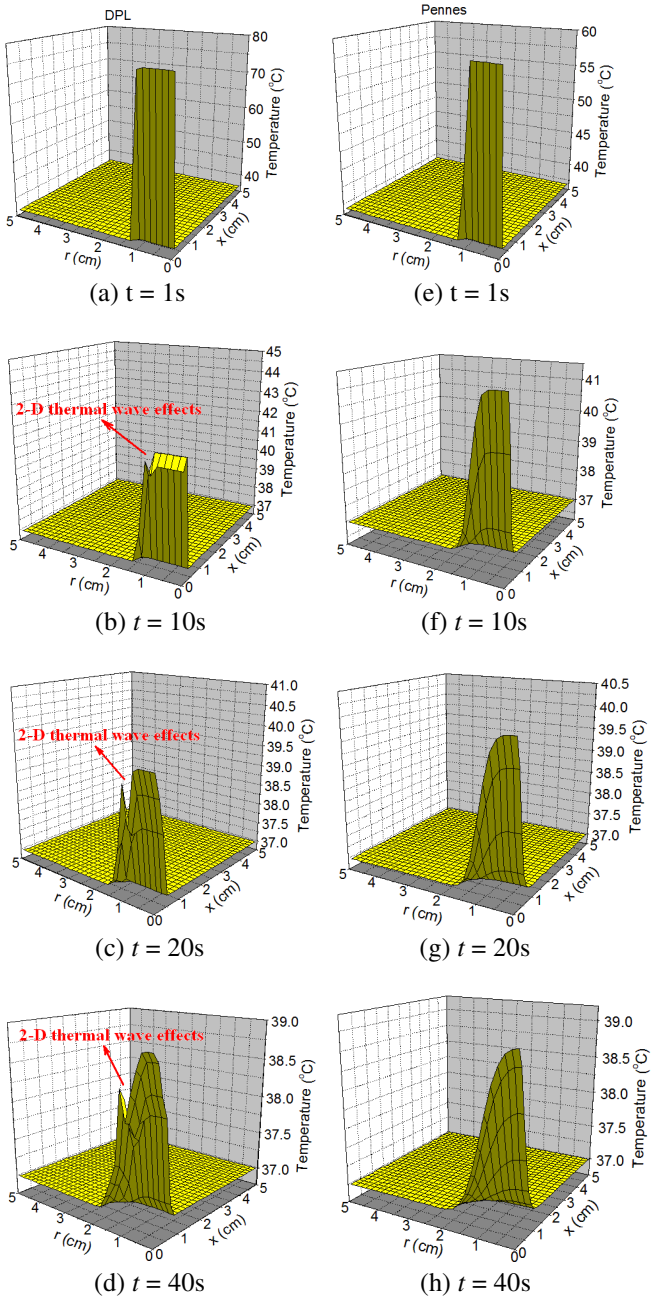

Figure 10 2D temperature distributions at different time instants for surface heating. (a)-(d) 2-D DPL model; (e)-(f) Traditional parabolic model.

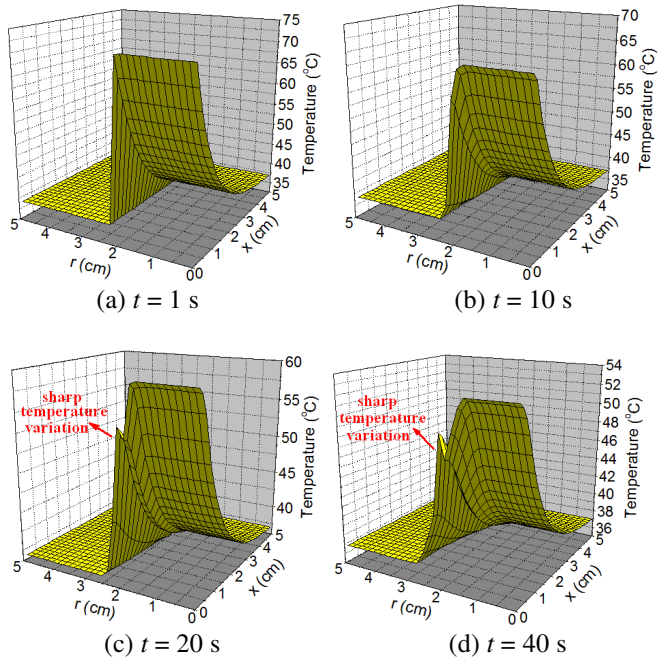

(a) t = 1 s (b) t = 10 s

(c) t = 20 s (d) t = 40 s

Figure 11 2D temperature distributions at different time instants for body heating. (a) t = 1 s; (b) t = 10 s; (c) t = 20 s; (d) t = 40 s.

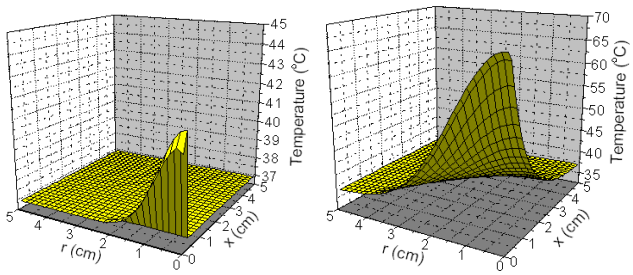

(a) Surface heating (b) Body heating

Figure 12 2D temperature distributions in the tissue heated by an incident Gaussian heat flux at t = 10s. (a) surface heating; (b) body heating.

The foregoing simulations are performed for tissues that are heated by a uniform incident heat flux. In real medical practices, the irradiations can be in Gaussian distribution. Figure 12 illustrates the 2D temperature distributions at t = 10 s for the tissue heated by an incident Gaussian heat flux $\Phi_{in} = \Phi_{in\max} \exp(-r^2 / r_p^2)$, where $\Phi_{in\max}$ = 4 W/cm^2 and r_p = 1 cm for the surface heating (Fig. 12 (a)) and $\Phi_{in\max}$ = 150 W/cm^2 and r_p = 2 cm for the body heating (Fig. 12 (b)). For the latter, the Beer's law is used again to describe the volumetric heat source distribution in the axial direction. The two lagging times used are τ_q = 8 s and τ_T = 0.5 s. As shown in Fig. 12, no thermal wave exhibits in the body heating case but in the surface heating case. Due to the non-uniform distribution of the incident heat flux, the 2D effect on the temperature transient is pronounced for both cases.

6. CONCLUSIONS

In this work, two non-Fourier heat conduction models, hyperbolic thermal wave model and dual-phase-lag model, are developed to investigate the thermal response of laser-irradiated biological tissues. The laser light propagation in tissues is determined by using the Beer's law, broad beam approach and seven flux method. The thermally induced damage in tissues is evaluated by using the rate equation for protein denaturation process. The calculating results computed with the hyperbolic thermal wave, DPL and Fourier's heat conduction models are compared. It is shown that the non-Fourier approaches predict significantly different temperature and thermal damage in tissues compared to the traditional Fourier's heat conduction models. It is also found that the DPL bioheat conduction equations can only be reduced to the Fourier heat conduction equations when both the phase lag times of the temperature gradient (τ_T) and the phase lag of the heat flux (τ_q) are zero. This is different from the DPL model for pure conduction materials, for which it is reduced to the Fourier's model as long as $\tau_q = \tau_T$. Parametric studies are also performed to examine the influences of the thermal relaxation and phase lag times and blood perfusion on the thermal damage progress in laser irradiated tissues. The result shows that the overall effects of the blood flow on the thermal response and damage are similar to those of the time delay τ_T. For local surface heating with a uniform incident heat flux, thermal wave exhibits in both the axial and radial directions, while it could only exhibit in the radial direction for a body heating. When the spot of a local heating is smaller than the tissue bulk size, the 2D effect may become pronounced, particularly for the region near the spot edge.

References

[1] H. H. Pennes, Analysis of tissue and arterial blood temperatures in the resting forearm, *Journal of Applied Physiology*, Vol. 1, pp. 93-122, 1948.

[2] K. J. Baumeister, and T. D. Hamill, Hyperbolic heat conduction equation-a solution for the semi-infinite body problem, ASME *Journal of Heat Transfer*, *Series C*, Vol.93, pp. 126–131, 1971.

[3] M. J. Maurer, and H. A. Thompson, Non-Fourier effects at high heat flux, ASME *Journal of Heat Transfer*, *Series C*, Vol.95, pp. 284–286, 1973.

[4] M. Chester, Second sound in solids, *Physical Review*, Vol. 131, pp. 2013–2015, 1963.

[5] M. S. Kazimi, and C. A. Erdman, On the interface

temperature of two suddenly contacting materials, ASME *Journal of Heat Transfer*, *Series C*, Vol.97, pp. 615–617, 1975.

[6] J. S. Rastegar, Hyperbolic heat conduction in pulsed laser irradiation of tissue, *Thermal and Optical Interactions with Biological and Related Composite Materials*, M. J. Berry and G. M. Harpole, Eds., *Proceedings of the SPIE*, Vol. 1064, SPIE Press, Bellingham, WA, pp. 114–117, 1989.

[7] W. Kaminski, Hyperbolic heat conduction equation for materials with a nonhomogeneous inner structure, ASME *Journal of Heat Transfer*, Vol.112, pp. 555–560, 1990.

[8] K. Mitra, S. Kumar, A. Vedavarz, and M. K. Moallemi, Experimental evidence of hyperbolic heat conduction in processed meat, ASME *Journal of Heat Transfer*, Vol.117, pp. 568–573, 1995.

[9] J. Liu, X. Chen, and L. X. Xu, New thermal wave aspects on burn evaluation of skin subjected to instantaneous heating, *IEEE Transactions on Biomedical Engineering*, Vol. 46, pp. 420-428, 1999.

[10] T. C. Shih, H. S. Kou, C. T. Liauh, and W. L. Lin, The impact of thermal wave characteristics on thermal dose distribution during thermal therapy: A numerical study, *Medical Physics*, Vol. 32, pp. 3029-3036, 2005.

[11] A. Banerjee, A. A. Ogale, C. Das, K. Mitra, and C. Subramanian, Temperature distribution in different materials due to short pulse laser irradiation, *Heat Transfer Engineering*, Vol. 26, No. 8, pp. 41-49, 2005.

[12] K. Kim, and Z. Guo, Multi-time-scale heat transfer modeling of turbid tissues exposed to short-pulsed irradiations, *Computer Methods and Programs in Biomedicine*, Vol. 86, pp. 112-123, 2007.

[13] C. Korner, and H. W. Bergmann, The physical defects of the hyperbolic heat conduction equation, *Applied Physics A*, Vol. 67, pp. 397-401, 1998.

[14] P. J. Antaki, New interpretation of non-Fourier heat conduction in processed meat, ASME *Journal of Heat Transfer*, Vol. 127, pp. 189-193, 2005.

[15] D. Y. Tzou, A unified field approach for heat conduction from macro- to micro-scales, ASME *Journal of Heat Transfer*, Vol.117, pp.8-16, 1995.

[16] D. Y. Tzou, Experimental support for the lagging response in heat propagation, AIAA *Journal of Thermophysics and Heat Transfer*, Vol. 9, pp.686-693, 1995.

[17] P. J. Antaki, New interpretation of non-Fourier heat conduction in processed meat, ASME *Journal of Heat Transfer*, Vol. 127, pp. 189-193, 2005.

[18] F. Xu, T. J. Lu, and K. A. Seffen, Biothermomechanical behavior of skin tissue, *Acta Mech Sin.*, Vol. 24, pp. 1-23, 2008.

[19] B. Shen, and P. Zhang, Notable physical anomalies manifested in non-Fourier heat conduction under the dual-phase-lag model, *International Journal of Heat and Mass Transfer*, Vol. 51, pp. 1713-1727, 2008.

[20] F. Xu, K. A. Seffen, and T. J. Liu, Non-Fourier analysis of skin biothermomechanics, *International Journal of Heat and Mass Transfer*, Vol. 51 pp. 2237-2259, 2008.

[21] H. Q. Yang, Solution of two-dimensional hyperbolic heat conduction by high-resolution numerical methods, *Numerical Heat Transfer, Part A*, vol. 21, pp.333-349, 1992.

[22] J. H. Zhou, D. Y. Liu, and J. Z. Xu, and X. L. Huai, Seven-flux modeling of laser light propagation in biological tissue in cylindrical coordinates (in Chinese), *Acta Photonica Sinica*, vol.31, no.6, pp. 662-667, 2002.

[23] A. J. Welch, and M. J. C. van Gemert, *Optical-Thermal Response of Laser-Irradiated Tissue*, Plenum Press, New York, 1995.

[24] C. M. Gardner, S. L. Jacques, and A. J. Welch, Light transport in tissue: accurate, heuristic expressions for one dimensional fluence rate and escape function based upon Monte Carlo simulations, *Lasers in Surgery and Medicine*, Vol. 18, pp. 129-138, 1996.

[25] G. Yoon, A. J. Welch, M. Motamedi, and M. C. J. van Gemert, Development and application of three-dimensional light distribution model for laser irradiated tissue, *IEEE Journal of Quantum Electronics*, vol.23, no. 10, pp. 1721-1732, 1987.

[26] J. H. Zhou, D. Y. Liu, and J. Z. Xu, and X. L. Huai, Seven-flux modeling of laser light propagation in biological tissue in cylindrical coordinates (in Chinese), *Acta Photonica Sinica*, vol.31, no.6, pp. 662-667, 2002.

[27] A. J. Welch, The thermal response of laser irradiated tissue, *IEEE Journal of Quantum Electronics*, Vol. 20, No. 12, pp. 1471-1481, 1984.

[28] Y. Yamada, T. Tien, and M. Ohta, Theoretical analysis of temperature variation of biological tissues irradiated by light, in: L. S. Fletcher, T. Aihara (Eds.), Proceedings of the *ASME/JSME Joint Thermal Engineering Conference*, Vol. 4, Amazon, Maui, Hawaii, 1995, pp. 575-581.

[29] W. F. Cheong, S. A. Prahl, and A. J. Welch, A review of the optical properties of biological tissues, IEEE *Journal of Quantum Electronics*, Vol.26, No.12, pp.2166-2185, 1990.